

Liquid-crystal based drift-free polarization modulators: Part II. Ultra-stable Stokes and Mueller polarimeters: supplement

JEAN REHBINDER,*  **JEAN DELLINGER, BRISÉIS VARIN,**  **MARC TORZYNSKI, YOSHITATE TAKAKURA, CHRISTIAN HEINRICH,**  **AND JIHAD ZALLAT** 

Laboratoire ICube, Université de Strasbourg, Bd Sébastien Brant, 67412 Illkirch, France

**rehbinder@unistra.fr*

This supplement published with Optica Publishing Group on 10 March 2023 by The Authors under the terms of the [Creative Commons Attribution 4.0 License](https://creativecommons.org/licenses/by/4.0/) in the format provided by the authors and unedited. Further distribution of this work must maintain attribution to the author(s) and the published article's title, journal citation, and DOI.

Supplement DOI: <https://doi.org/10.6084/m9.figshare.22110497>

Parent Article DOI: <https://doi.org/10.1364/OE.480774>

Liquid-crystal based drift-free polarization modulators - Part II. Ultra-stable Stokes and Mueller polarimeters: supplemental document

Simulating LCVR operation with an LCM. Figure S1 compares the evolution of the retardance of an LCM in its normal configuration (compensated temperature dependence) and in a setting simulating an LCVR ($\varphi_B=0$).

In this experiment, the temperature in the enclosure was set successively to 22, 38, and 50°C. The retardance of the LCM was measured for a set of φ_A and φ_B values.

The figure illustrates how the temperature-dependence vanishes at low retardance in the LCVR setting. It also shows the effectiveness of the LCM for obtaining stable retardance values over a wide temperature range.

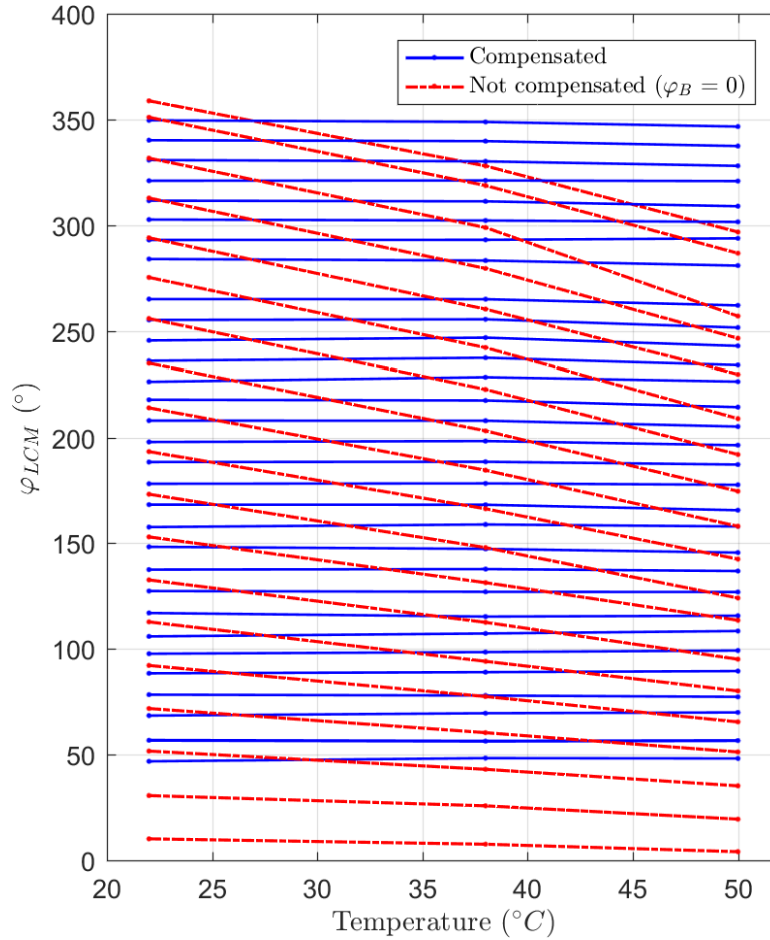


Fig. S1. Temperature dependence of the retardance of a LCM with compensation (LCM, blue lines) and without compensation (simulating a LCVR, red dotted lines).

Repeatability of the measurements. We compare two measurements with the same system (see section 3 and figure 3) and the same configuration as the experiments described in the main document. Measure 1 and measure 2 were performed at few days' interval.

Figure S2-S4 are counterparts to Figure 4-6 of the main document.

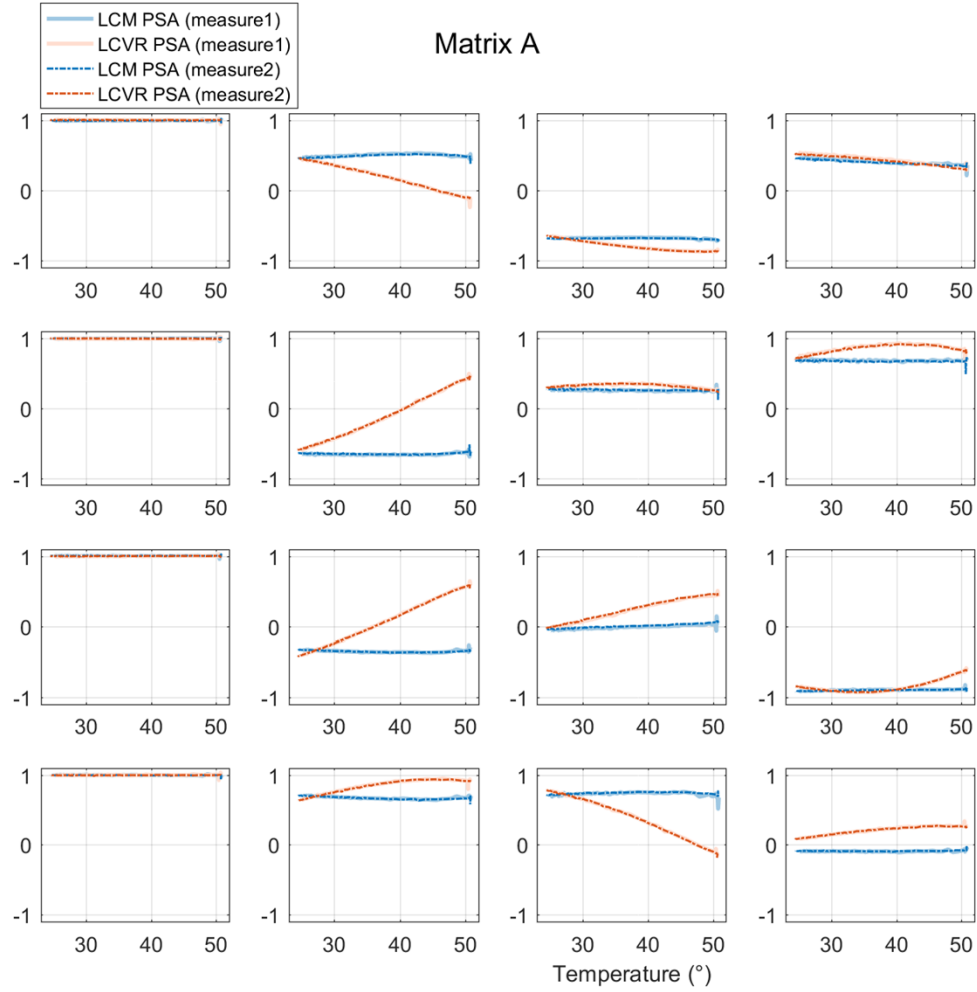


Fig. S2. Temperature dependence of the measurement matrix A of a PSA with compensation (LCM-PSA, blue lines) and without compensation (LCVR-PSA, red lines). Full lines of light color correspond to measure 1, dotted lines of darker color to measure 2.

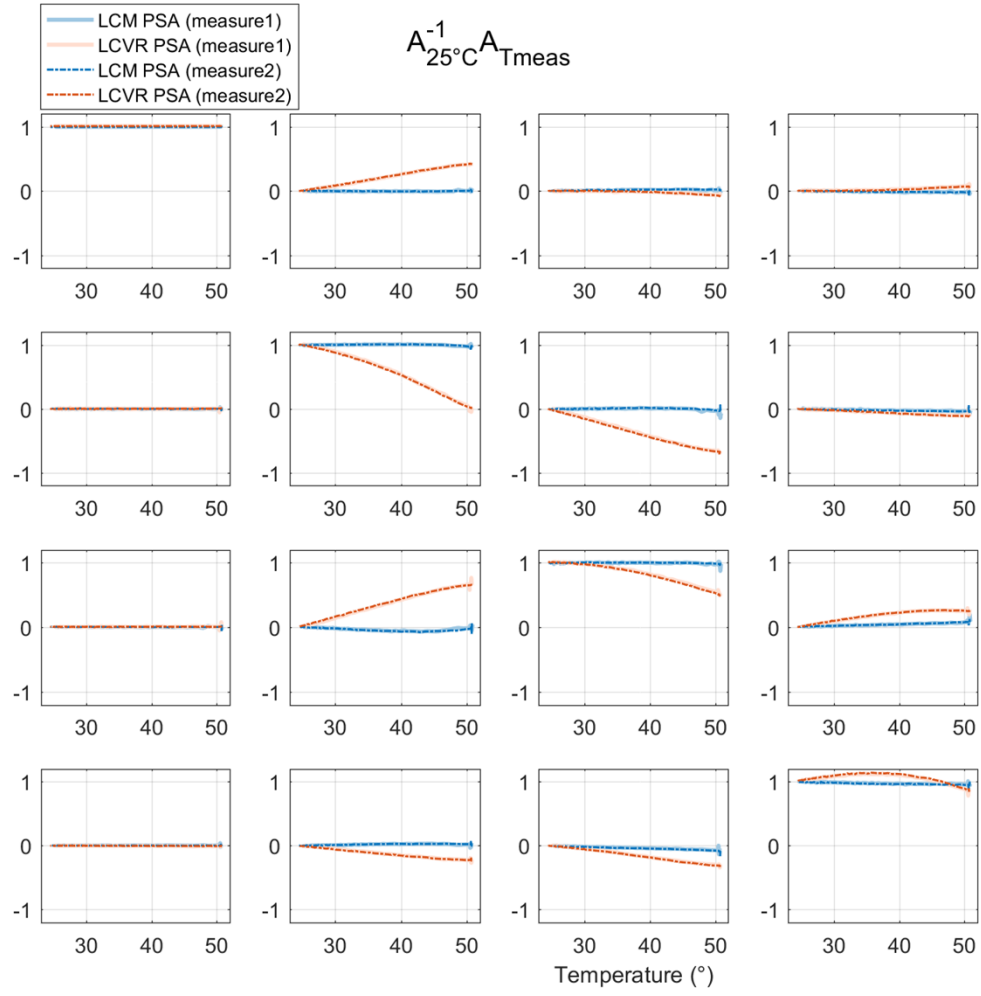


Fig. S3. Temperature dependence of the transfer matrix $A_{25^{\circ}\text{C}}^{-1} A_{T_{\text{meas}}}$ of a PSA with compensation (LCM-PSA, blue lines) and without compensation (LCVR-PSA, red dotted lines). Full lines of light color correspond to measure 1, dotted lines of darker color to measure 2.

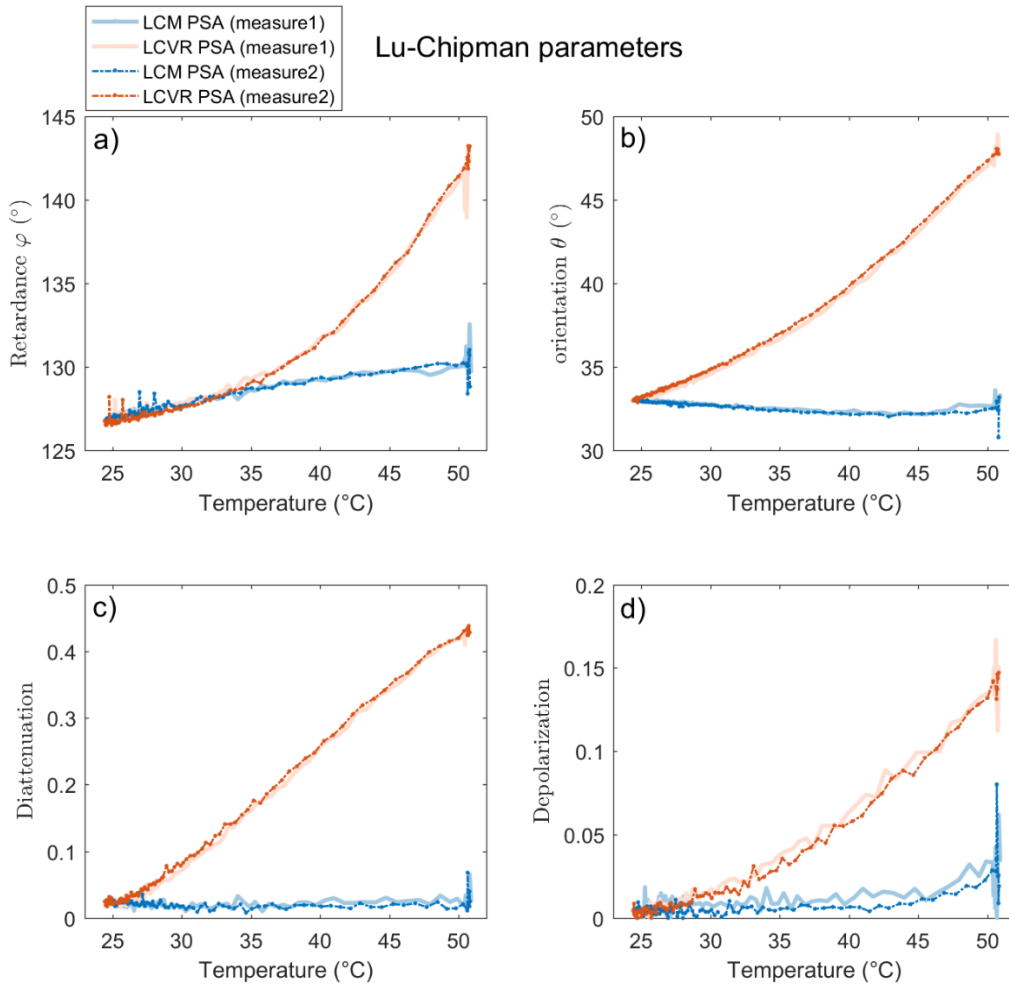


Fig. S4. Temperature dependent parameters of a waveplate obtained with compensated (LCM-PSA) and standard (LCVR-PSA) PSA in the Mueller configuration: (a) Retardance, (b) orientation of the retarder, (c) Diattenuation, and (d) Depolarization extracted from the Mueller matrix using polar decomposition